M2 macrophage-derived exosomes for DNase 1 delivery to modulate inflammatory microenvironment in ischemic stroke

Hongrui Qing
Southwest Jiaotong University
Zhenhua Wang
Southwest Jiaotong University
Ran Li
Southwest Jiaotong University
Xue Li
Southwest Jiaotong University
Xing Guo (xingguo@swjtu.edu.cn)
Southwest Jiaotong University
Shaobing Zhou
Southwest Jiaotong University https://orcid.org/0000-0002-6155-4010

Article

Keywords:

Posted Date: June 17th, 2022

DOI: https://doi.org/10.21203/rs.3.rs-1736246/v1

M2 macrophage-derived exosomes for DNase 1 delivery to modulate inflammatory microenvironment in ischemic stroke

Hongrui Qing[1], Zhenhua Wang[1], Ran Li[1], Xue Li[1], Xing Guo[1*] & Shaobing Zhou[1]

[1]Key Laboratory of Advanced Technologies of Materials, Ministry of Education School of Materials Science and Engineering, Southwest Jiaotong University, Chengdu 610031, China.

Corresponding author

Correspondence to: Xing Guo*

E-mail: xingguo@swjtu.edu.cn

Abstract

Neutrophil extracellular traps (NETs) are highly associated with inflammatory response and vascular injury after ischemic stroke. As the primary degrader of NETs, DNase 1 is limited by easy deactivation and low efficiency of crossing the blood-brain barrier (BBB). Here, we develop a M2 macrophage-derived exosomal (M2exo) system for DNase 1 delivery to achieve enhanced ischemic stroke therapy. The nanoplatform can cross the BBB through transcytosis of exosomes, subsequently clearing NETs by DNase 1 to inhibit inflammatory factors release and prevent vascular injury. Moreover, M2exo induced the polarization of M1 microglia to M2 phenotype, alleviating neuroinflammation via producing anti-inflammatory cytokines. This nanoplatform exhibits significant efficiency of reducing brain infarct area, improving long-term neurologic outcome, and promoting BBB remodeling. The mechanism for the synergistic effect from M2exo and DNase 1 is unveiled at the genetic level through transcriptome analysis. This work provides a paradigm of improving the effectiveness of ischemic stroke therapy.

Introduction

Stroke is the leading cause of death and long-term disability in the world, and ischemic stroke resulted from

cerebral artery thromboembolism accounts for about 87%, which is the most common type of stroke[1]. After ischemia, inflammation and immune response play key roles in the pathophysiology of stroke[2]. As the first group of cells to be recruited form the periphery to the brain after ischemia, neutrophils are highly involved in inflammation post stroke[3]. When neutrophils accumulate at the ischemic area, reactive oxygen species (ROS) generated by NADPH oxidase or mitochondria can promote the depolymerization of neutrophil chromatin by activating myeloperoxidase (MPO), neutrophil elastase (NE) and peptidylarginine deiminase 4 (PAD4)[4]. Subsequently, the activated neutrophils release nuclear and granular contents to form web-like structures of DNA, which are known as neutrophil extracellular traps (NETs). NETs can regulate inflammatory cytokines directly or indirectly by modulating other immune cells[4,5]. NETs-mediated inflammatory response recruits pro-inflammatory cells and proteins to form immune complexes that induce autoantibody production, leading to tissue damage[6]. The pro-inflammatory role of NETs has been previously documented in ischemia-reperfusion injury and autoimmune diseases including psoriasis, rheumatoid arthritis, and systemic lupus erythematosis[6,7]. Despite the inflammatory reactions, NETs have been proved to impair revascularization and vascular remodeling after stroke[8]. Furthermore, NETs can also contribute to coagulation, vascular occlusion and thrombosis[9,10]. Therefore, degrading NETs can reduce brain infarct and improve neurofunctional recovery through alleviating inflammation, promoting vascular remodeling and preventing thrombosis. DNase 1 has been identified as the primary degrader of NETs, however, it is limited by short half-life in blood circulation and low efficiency to cross the blood-brain barrier (BBB)[11].

In addition to inflammation, immune response exhibits a significant influence on the pathogenesis and prognosis of stoke. As resident immune cells in the brain, microglia are the first defense line of central nervous system (CNS) against pathogen invasion and the first non-neural cells responding to acute ischemic stroke (AIS). Microglia are in resting state (M0 type) under physiological condition and play the role of “immune surveillance”. After cerebral ischemia, microglia can be activated and polarized into either the “classically activated” M1 phenotype or“alternatively activated” M2 phenotype[12]. Activated microglia play a dual role in CNS, functioning as neurotoxicity or neuroprotective according to different polarization

phenotypes[13]. M1 microglia secrete inflammatory cytokines to cause tissue damage. In contrast, M2 microglia produce anti-inflammatory cytokines, exerting neuroprotective effect by inhibiting nerve injury and promoting tissue repair[14]. Therefore, inducing microglia to M2 polarization can effectively repair the damaged nerve and improve long-term neurological outcomes.

In recent years, exosomes, which are cell-derived membrane-bound vesicles with diameters of 30 ~ 150 nm, have been widely studied as both delivery carriers and therapeutics for stroke treatment[15]. As carriers for delivering cargo to infarcted brain, exosomes can cross the BBB, infiltrate the CNS, and accumulate around the ischemic lesion[16,17]. As therapeutics, exosomes enriched with microRNAs (miRNAs) have been shown to benefit neurite remodeling, regulate neuronal excitability and reduce infarct volume when employed to treat AIS[15]. Furthermore, it is well documented that exosomes derived from the M2 phenotype macrophages (M2exo) can secrete anti-inflammatory cytokines, leading to M2 polarization in immune cells[18]. Increasing evidences have demonstrated that M2exo can be used as drug delivery systems to treat rheumatoid arthritis, atherosclerosis and cancer[19-21]. However, few studies of M2exo have focused on their phenotype regulatory function in ischemic stroke.

Herein, we report a new strategy by utilizing DNase 1-loaded M2exo (M2exo@DNase 1) for ischemic stroke treatment. The nanoplatform can cross the BBB *via* exosomes-mediated transcytosis, followed by accumulating around the ischemic area. With the secretion of anti-inflammatory cytokines by M2exo, microglia can be polarized into M2-phenotype, exerting neuroprotective effect. Furthermore, DNase 1 released from the exosomes can degrade NETs to reduce inflammation and promote vascular remodeling. To simultaneously induce M2 polarization of microglia and clearance of NETs, M2exo@DNase 1 provides a prospective approach for tissue repair in ischemia-reperfusion injury.

Results

Preparation and characterization of M2exo@DNase 1. To prepare DNase 1-loaded M2exo, RAW264.7 were first polarized to M2 phenotype by IL-4. The phenotypic change was investigated by measuring the surface markers of macrophage and analyzing the secretion of cytokines, including tumor necrosis factor

(TNF-α), interleukin-6 (IL-6), interleukin-10 (IL-10) and transforming growth factor-β (TGF-β). The population of CD11b+CD206+-labeled M2 macrophages treated with IL-4 was approximately 70% by flow cytometry analysis (Supplementary Fig. 1). Compared with untreated RAW264.7, antiinflammation factors IL-10 and TGF-β showed remarkable enhanced secretion, by contrast, proinflammatory factors TNF-α and IL-6 displayed reduced secretion (Supplementary Fig. 2). These results indicated that RAW264.7 could be successfully polarized to anti-inflammatory M2 phenotype. Then M2exo were collected by gradient centrifugation of the cell supernatant, followed by encapsulation of DNase 1 into the exosomes via electroporation to obtain M2exo@ DNase 1.

Transmission electron microscopy shows the typical cup-shaped membrane vesicle morphology of M2exo@DNase 1 (Fig. 1a). The particle sizes of M2exo and M2exo@DNase 1 were 135.8 nm and 143.2 nm, respectively (Supplementary Fig. 3). Besides, the zeta potential of M2exo@DNase 1 (-15.3 mV) was similar to M2exo (-15.6 mV) (Supplementary Fig. 4). Compared with RAW264.7 membrane, the protein content of M2exo was 2.3-fold higher, indicating more abundant protein of exosomes (Supplementary Fig. 5). There was no significant difference in protein expression between M2exo and M2exo@DNase 1 (Supplementary Fig. 6), suggesting that the nature of exosomes was not affected by the encapsulation of cargo. These results together illustrated the successfully fabrication of M2exo@DNase 1. Next, we measured the drug loading efficiency of M2exo@DNase 1 to be 81.75% with loading content of 1422 U/mg. Compared with DNase 1, M2exo could increase 58% of enzymatic activity at 48 h, preventing early inactivation of DNase 1 (Supplementary Fig. 7).

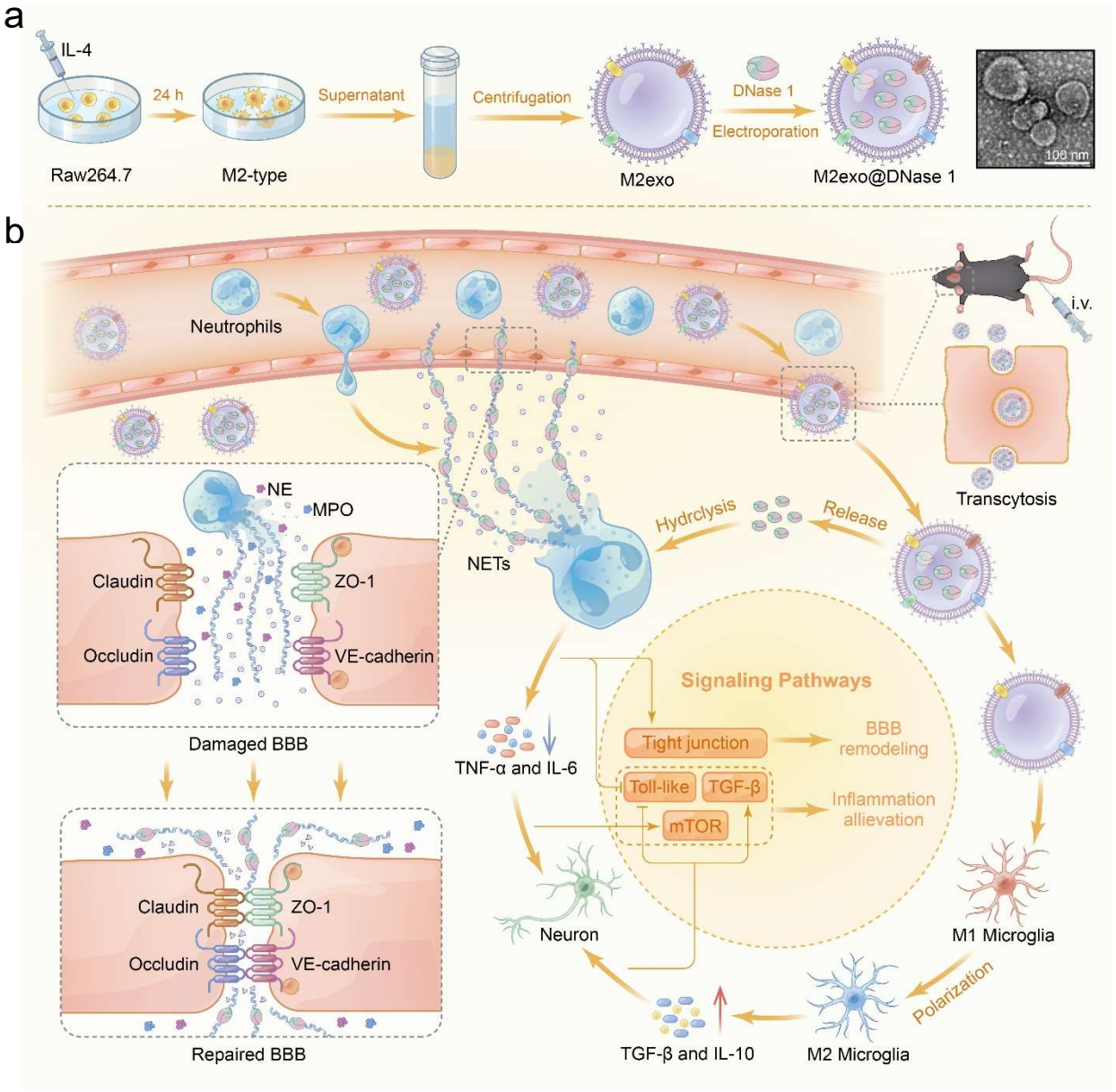

Fig. 1 Schematic illustration of M2exo@DNase 1 therapy for ischemic stroke. a Scheme of the M2exo@DNase 1 preparation process. RAW264.7 were treated with IL-4 to be polarized into M2 phenotype, and the supernatant was collected to be centrifuged to obtain M2exo. M2exo@DNase 1 was fabricated by encapsulation of DNase 1 into M2exo through electroporation. Transmission electron microscopy shows the typical cup-shaped membrane vesicle morphology of M2exo@DNase 1. **b** Illustration of the M2exo@DNase 1 therapy and signaling pathways involved in the process. M2exo@DNase 1 entered the ischemic brain through transcytosis of exosomes. DNase 1 released from the

exosomes degraded NETs to inhibit inflammatory factors and promote BBB remodeling. In the meantime, M2exo induced the conversion of M1 microglia to M2 type, exerting neuroprotective effect. This process is involved in downregulation of Toll-like signaling and mTOR signaling, and upregulation of tight junction signaling and TGF-β signaling.

In vitro microglia polarization and NETs inhibition. To investigate the effect of M2exo on microglia polarization, microglia were first applied under OGD/R condition to be converted to M1 phenotype. After treating with M2exo, microglia exhibited M2-type ratio of 64.3%, which was 5.4-fold that of PBS group (Fig. 2a, b). In contrast, negligible change was observed in the cells by M0exo treatment, indicating that there's no impact of inactivated exosomes on microglia polarization. Remarkably, the polarization efficiency of M1 to M2 was a little bit decrease in M2exo@DNase 1 group. We speculate that this is caused by interference of DNase 1 with the process of exosomal miRNA reverse transcription[22].

Then we evaluated whether M2exo@DNase 1 could decompose NETs in vitro. Neutrophils were first extracted from mouse bone marrow and treated with phorbol 12-myristate 13-acetate (PMA) to induce the formation of NETs. The extracted neutrophils were identified by Wright's stain, which showed multinucleated cell structure (Supplementary Fig. 8). Besides, the flow cytometry analysis indicated that the purity of these cells was as high as 90.4% (Supplementary Fig. 9). To investigate whether NETs were produced by PMA trigger, neutrophils were stained with citrullinated histone H3 (H3Cit, key protein involved in the formation of NETs) and observed by fluorescence microscopy. We found significant H3Cit fluorescence was expressed by PMA-induced neutrophils, indicating successful generation of NETs (Fig. 2c). Next, we explored the inhibitory effect of M2exo@DNase 1 on NETs. After treating the PMA-induced neutrophils with DNase 1, the reticular structure of NETs by SYTOX Green stain disappeared (Fig. 2d). Notably, M2exo@DNase 1 could also reduce SYTOX green-positive extracellular DNA fibers, the number of NETs in which was comparable to DNase 1 group (Fig. 2e). Quantitative fluorescence analysis revealed that NETs were disassembled by 38.6% within 15 min (Supplementary Fig. 10). Moreover, the NETs

components including NETs, eDNA and neutrophil elastase (NE) were remarkably reduced by M2exo@DNase 1 treatment (Fig. 2f), which was consistent with the H3Cit and SYTOX Green stain.

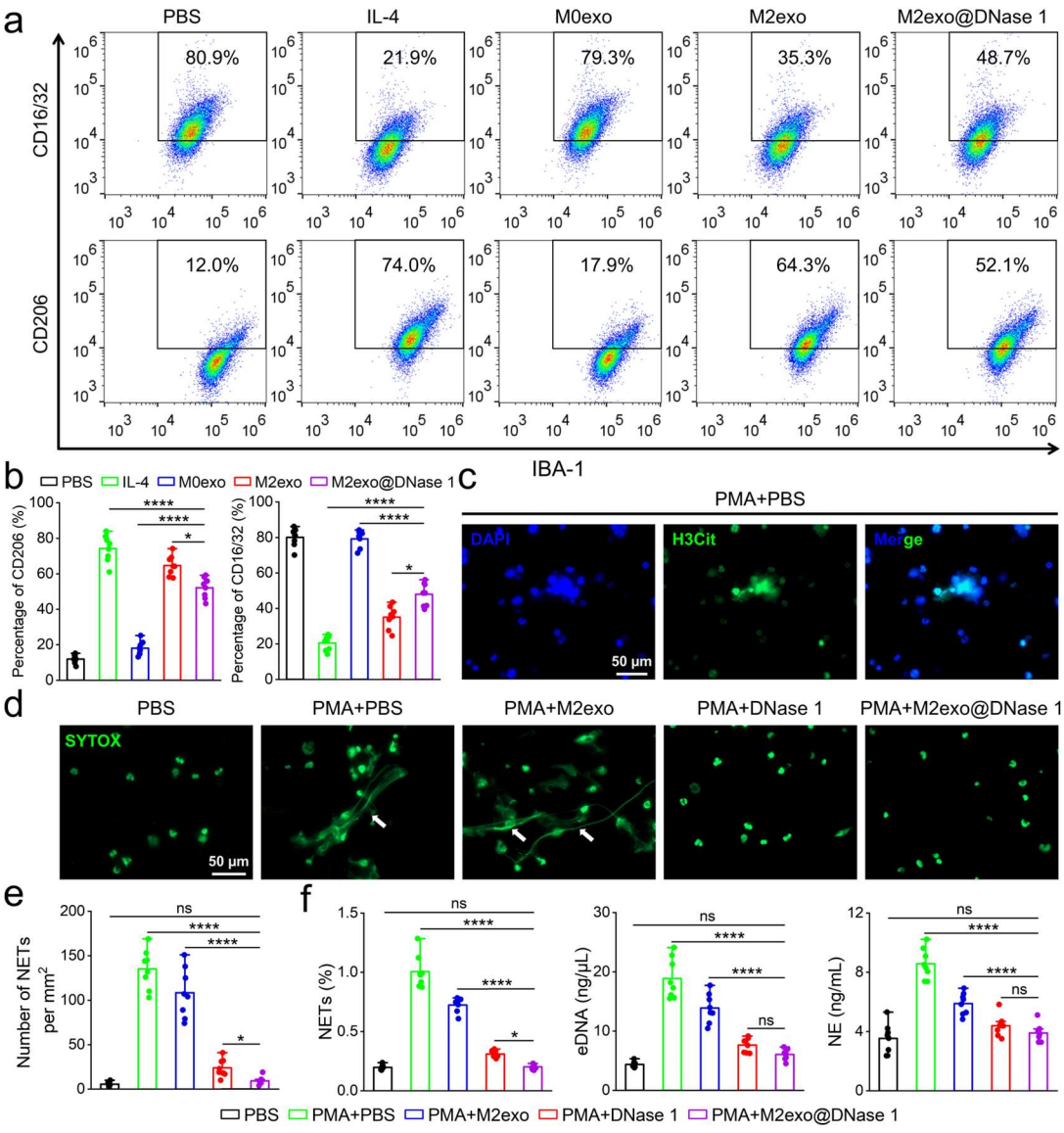

Fig. 2 In vitro microglia polarization and NETs inhibition by M2exo@DNase 1. a Representative flow cytometry plot of the M1-type microglia (labeled with IBA-1$^+$CD16/32$^+$) and M2-type microglia (labeled with IBA-1$^+$CD206$^+$) among microglia treated with different formulations. **b** Percentages of IBA-1$^+$CD206$^+$ and IBA-1$^+$CD80$^+$ cells within microglia, n = 8/group. **c** Representative fluorescence images of H3Cit (green) showing NETs formation by PMA-induced neutrophils. Nucleus were stained with DAPI (blue). **d**

Representative fluorescence images of extracellular DNA (Sytox, green) in neutrophils with or without PMA trigger followed by treatment with different formulations. The extracellular DNA fibers showing NETs formation were indicated with white arrows. **e** Quantification of NETs according to SYTOX-stained fluorescent images, *n* = 8/group. **f** Levels of NETs, eDNA and NE measured by ELISA, *n* = 8/group.

In vivo therapeutic effects on MCAO model. To explore whether M2exo would induce the long-term retention and enrichment of cargo in the infarct brain, mice after middle cerebral artery occlusion (MCAO) surgery were intravenously injected with indocyanine green (ICG)-loaded M2exo (M2exo@ICG) and then monitored using near-infrared fluorescence in vivo imaging system (IVIS). Compared with ICG group, mice treated with M2exo@ICG exhibited stronger fluorescence signals at the ischemic hemisphere at 1 h, 3 h, 6 h and 12 h post-injection (Fig. 3a), which could be due to the enhanced BBB permeability and prolonged retention of exosomes. Quantitative analysis of mean radiant efficiency showed that the fluorescence intensity of the infarct brain of M2exo@ICG-treated mice was approximately 5.6-fold higher than that in the ICG group at 12 h (Fig. 3b). Moreover, ex vivo imaging at 12 h post-injection clearly indicated more intense fluorescence signals in the ischemic brain of the mice in the M2exo@ICG group (Fig. 3c, Supplementary Fig. 11).

Real-time monitoring of cerebral blood flow is an effective approach to evaluate the severity of ischemia in stroke lesions and can be used to characterize reperfusion injury[23]. To explore whether M2exo@DNase 1 produce therapeutic benefit for MCAO mice, laser speckle contrast imaging system was applied to monitor the regional cerebral blood flow (rCBF) of mice before, after surgery and after treatment. As shown in Fig. 3d, the color-coded images of blood flow showed rCBF decline by ~80% after MCAO surgery, illustrating the consistency of ischemia among groups. The blood flow of mice recovered to 91.9% after M2exo@DNase 1 treatment, which was approximately 1.2-fold higher than that of MCAO group (Fig. 3e), indicating enhanced recanalization of blood vessels. The TTC staining of brain sections visually revealed the brain injury of MCAO mice. Treatment with DNase 1 or M2exo shrank the infarct area of 12.9% and

39.9% in contrast to MCAO group, whereas M2exo@DNase 1 therapy reduced 71.2% of infarction (Fig. 3f, g).

Then we determined the impact of treatment with different formulations on brain edema. By measuring the dry and wet weight of mice brains, the water content in the ipsilateral hemispheres in M2exo@DNase 1 group was 79.7%, which is significantly lower than that in MCAO group (81.9%) (Fig. 3h). To investigate the long-term variation of brain lesion poststroke, MRI was performed on day 3, 7, 14 and 28 after MCAO surgery. Significant brain lesion was observed from the T2-weighted cerebral MRI images of MCAO mice during the experimental period (Fig. 3i). Treatment with M2exo or DNase 1 exhibited weak recovery of brain injury. In contrast, M2exo@DNase 1 therapy resulted in remarkable shrinkage of brain lesion area, reducing 74% of infarct volume when comparing with MCAO group on day 28 (Supplementary Fig. 12). The result indicated efficient alleviation of long-term brain damage by the synergistic effect of NETs clearance and microglia polarization. Pathological examination of the mice brains by hematoxylin-eosin (H&E), Nissl and luxol fast blue (LFB) staining demonstrated that M2exo@DNase 1 exhibited better recovery of neuronal functions than other groups (Fig. 3j).

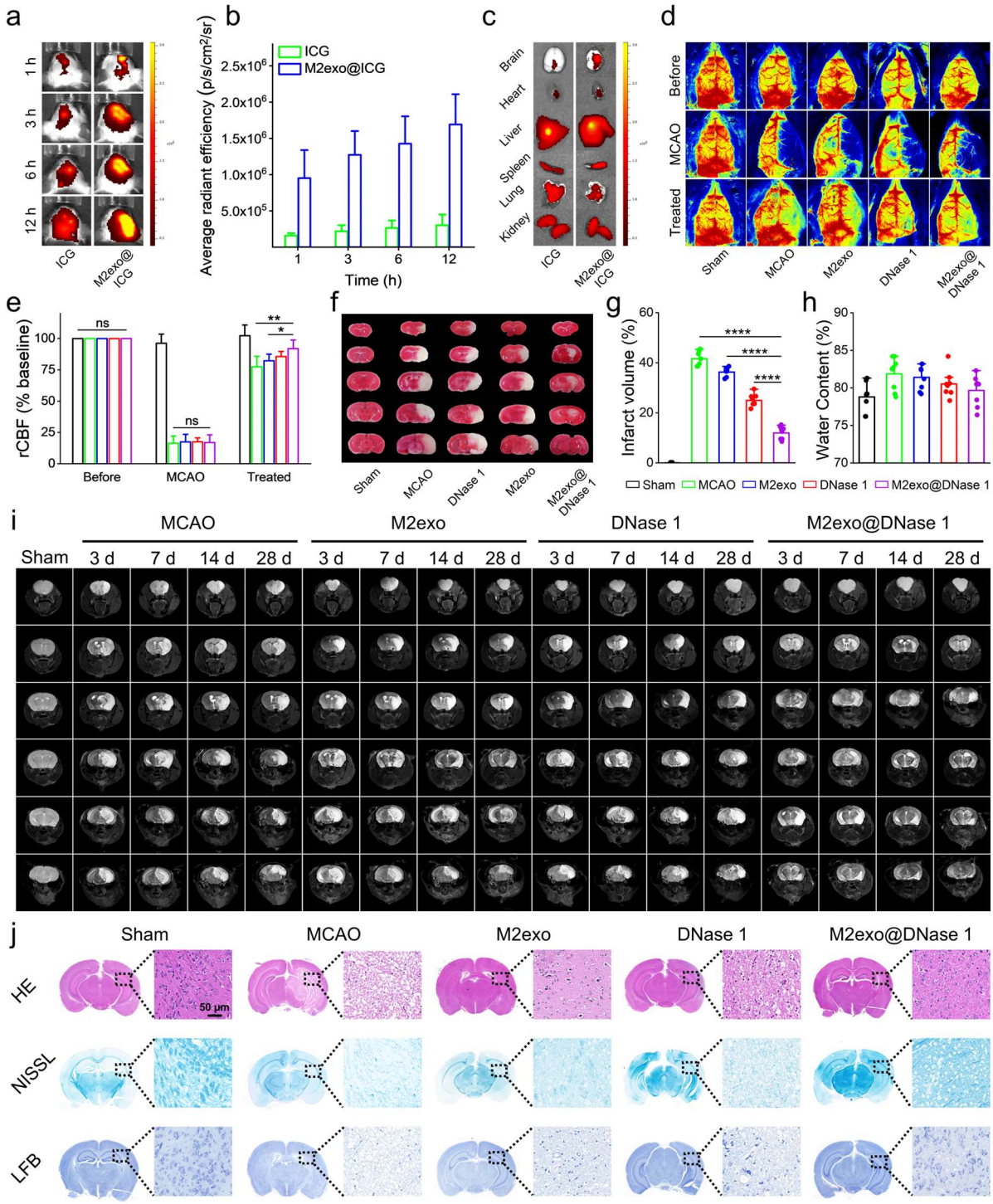

Fig. 3 Biodistribution and therapeutic effect against MCAO mice. a In vivo fluorescence imaging of ICG and M2exo@ICG in the mice brain. **b** The average radiation efficiency of ICG and M2exo@ICG in the mice brains based on fluorescence intensity, *n* = 3/group. **c** Ex vivo fluorescence imaging of ICG and

M2exo@ICG in the mice tissues. **d, e** rCBF of sham or MCAO mice treated by M2exo, DNase 1 and M2exo@DNase 1 before, after surgery and after treatment, *n* = 3/group. **f, g** Representaive images of TTC-stained brain slices and quantification of infarct size in mice brains at 3 d after MCAO. **h** Brain water content of mice at 3 d after MCAO, *n* = 8/group. **i** MRI images showing brain infarction at 3, 7, 14 and 28 d after MCAO. **j** Images of HE, NISSL and LBF-stained brain slices at 3 d after MCAO.

M2exo@DNase 1 improves long-term neurological functional outcome. To explore the impact of M2exo@DNase 1 on long-term motor and cognitive function recovery of MCAO mice, behavioral tests were performed from pre-surgery (Pre) to day 28 poststroke. The rotarod, cylinder, adhesive, and beam balance tests as well as the modified neurological severity score (mNSS) demonstrated that MCAO surgery destroyed sensorimotor function of mice during 28 days post operation (Fig. 4a-h, Movie S1). MCAO mice that received M2exo@DNase 1 experienced earlier and sustained improved recovery with significant reversed neurological deficits. Cognitive function was assessed by Barnes maze test. In the late phase of day 28, path length and escape latency/number of errors were recorded to evaluate the spatial learning ability of mice. The results showed that MCAO mice spent more time and longer distance to find the escape hole than sham mice (Fig. 4i-k). In contrast, M2exo@DNase 1 mice exhibited obvious alleviated spatial learning deficits, as indicated by shorter time and fewer errors to find the escape hole. The behavioral results indicated that M2exo@DNase 1 therapy promoted the long-term neurofunctional outcome for stroke. To evaluate whether there's a correlation between neurological function and cerebral infarction, a linear fit was performed. We found that most of the behavioral results were correlated well with the infarct volume from TTC staining, suggesting that the brain injury can be reflected by the neurological function (Fig. 4l). Given the superior therapeutic effect and reversed neurological deficits, M2exo@DNase 1 mice possessed survival rate of 80% at day 28 poststroke, which was 50% higher than MCAO mice (Fig. 4m).

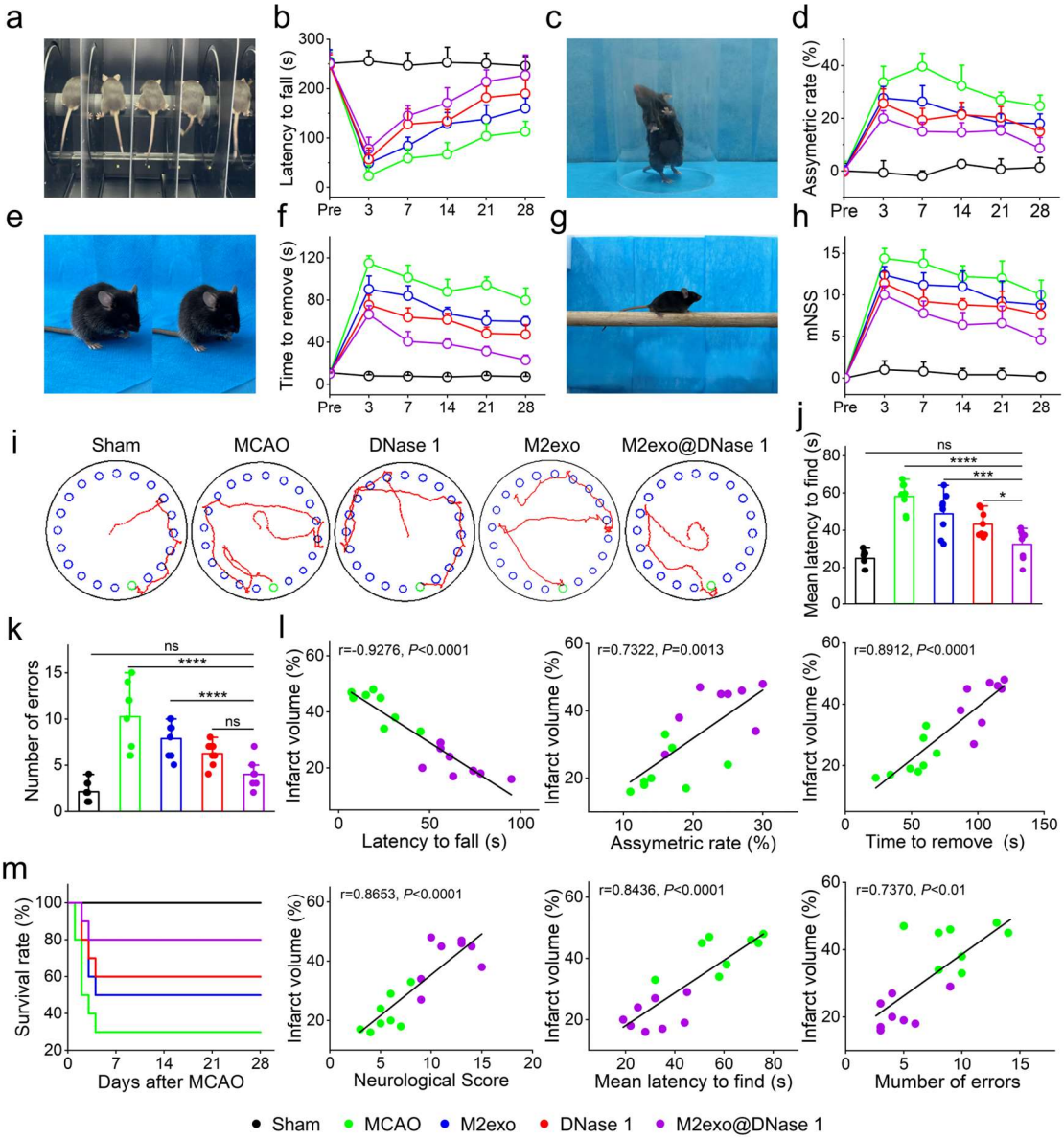

Fig. 4 Long-term neurological functional outcome. a Digital photo of rotary test. **b** Latency to fall in the rotarod test. **c** Digital photo of cylinder test. **d** Forelimb asymmetry rate in the cylinder test. **e** Digital photo of adhesive test. **f** Time to remove the tape in the adhesive test. **g** Digital photo of beam balance test. **h** mNSS including the motor test, the sensory test, the beam balance test, reflex loss and abnormal movement. **i** The motion path of mice in the Barnes maze test. **j** Mean latency to find the escape hole and **k** number of errors in the Barnes maze. *n* = 8/group for the behavioral tests. **l** Linear fit of infarct volume from the TTC

staining and latency to fall, asymmetric rate, time to remove, neurological score, mean latency to find and number of errors at 3 days post MCAO. **m** Survival rate of mice in different groups, n = 10/group.

In vivo microglia polarization and NETs inhibition. For in vivo microglia polarization study, immunofluorescence staining was first performed. As shown in Fig. 5a, negligible CD16/32 or CD206 expression was observed from sham mice, indicating that microglia were in resting state (M0 type) under physiological condition. MCAO surgery led to abundant CD16/32 expression, suggesting the transition of M0 microglia to M1 phenotype upon ischemic injury. Owing to the anti-inflammatory effect of the exosomes derived from M2 microglia, M2exo group exhibited fewer CD16/32 while more CD206 expression than MCAO group. Interestingly, mice with M2exo@DNase 1 therapy resulted in most efficient M2 microglia polarization among all groups, which is different from the in vitro study (Fig. 2a). We assumed that this phenomenon was caused by the synergistic effect of inflammation alleviation through degrading NETs, further promoting the polarization of microglia to M2 type. The population of IBA-1^{+}CD206^{+} cells in M2exo@DNase 1 group was counted to be 34.2% for flow cytometry test, which was 1.3- and 2.1-fold that of M2exo and DNase 1 group, while MCAO group only counted to be 13.6% (Supplementary Fig. 13 and Fig. 14). Additionally, M1 microglia related cytokines (TNF-α, IL-6) and M2-type related cytokines (IL-10, TGF-β) in mice infarct brains were measured by ELISA kit. MCAO group had higher concentration of TNF-α and IL-6, and lower concentration of IL-10 and TGF-β, when comparing with other groups (Fig. 5b). M2exo@DNase 1 significantly increased the secretion of IL-10 and TGF-β, which were 2.1- and 1.3-fold that of MCAO group, respectively.

To explore the NETs inhibitory effect of M2exo@DNase 1, we first examined the extravasation of neutrophils in the mice brains using two-photon confocal microscopy. As shown in Fig. 5c, Ly6G-labeled neutrophils abundantly infiltrated into the peri-infarct cortex of MCAO mice, whereas these cells were almost undetectable in the sham mice. Additionally, immunostaining demonstrated that neutrophils were visualized throughout the infarct hemisphere in MCAO mice but not after sham surgery (Fig. 5d). Next, we investigated whether NETs were produced in the ischemic brain followed by neutrophil infiltration.

Immunostaining revealed that the ischemic brain section was extensively labeled with H3Cit in MCAO mice (Fig. 5e). Treatment with M2exo@DNase 1 did not affect the number of Ly6G-labeled neutrophils but reduced H3Cit expression. Consistent with this finding, western blot analysis of the ischemic brains showed increased H3Cit level in MCAO mice, which was greatly reduced by M2exo@DNase 1 treatment, showing 87.7% downregulation of H3Cit expression (Fig. 5f, Supplementary Fig. 15). We then determined the NETs components of the infarcted hemispheres using ELISA kit. Compared with MCAO group, M2exo@DNase 1 group reduced 55.8%, 87.1%, and 61.1% expressions of NE, NETs, and MPO levels, respectively (Fig. 6g). As NETs was found to activate the STING pathway and thus promoted inflammatory signaling in microglia[8,24]. we then asked whether M2exo@DNase 1 could contribute to STING inhibition. Western blot analysis of the ischemic cortex indicated a marked increase in the level of STING in mice subjected to stroke (Supplementary Fig. 16). Treatment with M2exo@DNase 1 resulted in remarkable decrease of STING expression, reducing 70.7% of STING level in comparison with MCAO group (Supplementary Fig. 17). Together, these findings suggest that NETs could be effectively disrupted by DNase 1-loaded exosomes derived from M2 microglia.

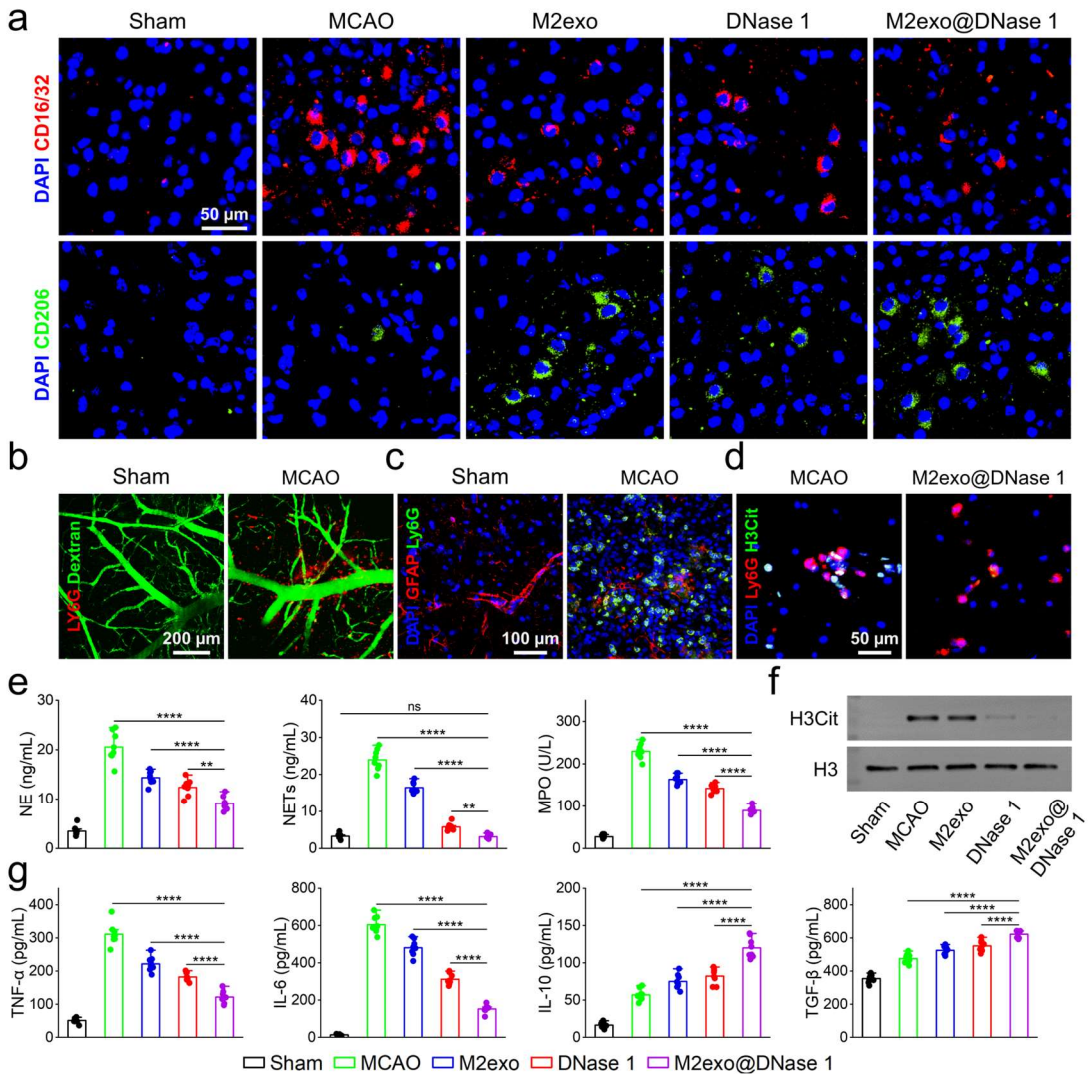

Fig. 5 In vivo microglia polarization and NETs inhibition by M2exo@DNase 1. a Representative CLSM images of M1 microglia (CD16/32$^+$, red) and M2 microglia (CD206$^+$, green) in different groups. Nucleus were stained with DAPI (blue). **b** In vivo two-photon imaging showing neutrophil aggregation in the MCAO mice brain. Blood vessels were imaged by intravenously injection of FITC-dextran (MW = 2000 kDa, green). Neutrophils were labeled with PE-Ly6G (red). **c** Representative CLSM images of astrocytes (GFAP$^+$, red) and neutrophils (Ly6G$^+$, green) in the mice brain. Nucleus were stained with DAPI (blue). **d** Representative CLSM images showing NETs (H3Cit, green) clearance after M2exo@DNase 1 treatment. Neutrophils were labeled with Ly6G (red) and nucleus were stained with DAPI (blue). **e** Levels of NE,

NETs and MPO in different groups measured by ELISA, *n* = 8/group. **f** Western blot of H3Cit in the infarct brains. **g** The cytokine levels of TNF-α, IL-6, IL-10 and TGF-1β in different groups, *n* = 8/group.

M2exo@DNase 1 promotes BBB remodeling after stroke. Encouraged by the efficient microglia polarization and NETs inhibition of M2exo@DNase 1, we next evaluated whether this combination effect could contribute to vascular remodeling after stroke. As a dye that can cross the damaged BBB but not the intact BBB, Evans blue was first performed to investigate the integrity of BBB. No extravasation of Evans blue occurred in the Sham group while abundant dye extravasation was observed in MCAO group (Fig. 6a), suggesting BBB was seriously destroyed poststroke. Notably, the infiltration of Evans Blue was reduced by 57.6% after treatment with M2exo@DNase 1 (Fig. 6b), indicating effective recovery of damaged BBB. Using two-photon microscopy to observe the cranial window of mice after intravenous injection of FITC-dextran, we found a significant increase in vascular leakage in the infarct areas of MCAO mice (Fig. 6c). The dye leakage could be partially suppressed in M2exo or DNase 1 group, showing 14.8% and 44.3% decrease of BBB permeability when comparing with MCAO group (Supplementary Fig. 18). Owing to the synergistic effect, mice treated with M2exo@DNase 1 exhibited a 65.6% reduction in BBB permeability. Consistent with this finding, the brain sections of ischemic areas confirmed the vascular remodeling ability of M2exo@DNase 1 (Fig. 6d).

To further evaluate the BBB integrity at the cytoarchitectural level, TEM was used to observe the infarct hemispheres of MCAO and M2exo@DNase 1 mice. The typical characteristics of damaged BBB was found in the TEM image of MCAO group, including mitochondrial swelling, dissolution of basement membrane, and disruption of tight junctions (Fig. 6e). In contrast, M2exo@DNase 1 therapy significantly shortened the vascular gap and restored the tight junctions. Western blot analysis revealed a significant increase in tight junction-related proteins including VE-cadheri, Claudin-5, Occludin and ZO-1 in M2exo@DNase 1 group, with approximately 2-fold increased expressions in infarct brains compared with MCAO group (Fig. 6f, Supplementary Fig. 19). Using ELISA, we confirmed that the proinflammatory IL-1β could be greatly

reduced by M2exo@DNase 1 therapy, which increased anti-inflammatory SOD and GSH-Px content in the infarct brains (Fig. 6g).

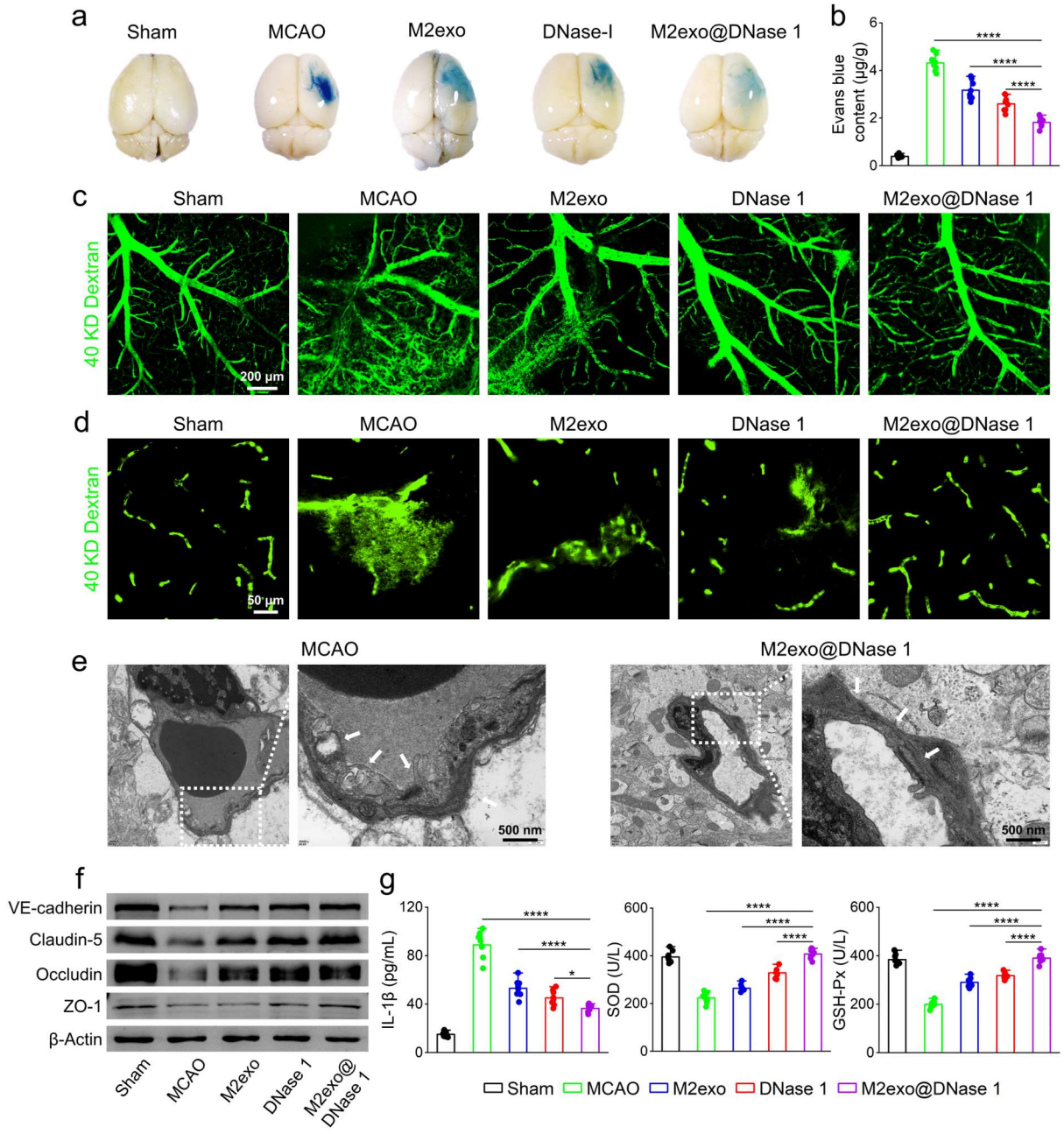

Fig. 6 M2exo@DNase 1 promotes BBB remodeling after stroke. a Digital photos showing Evans blue extravasation from the damaged BBB. **b** Quantitative analysis of Evans blue content in different groups, *n* = 8/group. **c** In vivo two-photon imaging of intravenously injected FITC-dextran (MW = 40 kDa, green)

leakage in cortical vessels. **d** CLSM images showing vascular extravasation of intravenously injected FITC-dextran (MW = 40 kDa, green). **e** TEM images showing the damaged BBB in MCAO group and repaired BBB in M2exo@DNase 1 group. The tight junctions on the BBB are pointed by white arrows. **f** Western blot of VE-cadherin, Claudin-5, Occludin and ZO-1 in mice brains. **g** The cytokine levels of IL-1β, SOD and GSH-Px in mice brains, *n* = 8/group.

Transcriptomic gene analysis. To figure out the molecular mechanism for the synergistic effect of microgila polarization and NETs inhibiton, we performed a transcriptome analysis. As shown in Fig. 7a, cluster analysis of differential gene expressions between Sham and MCAO indicated that a total of 2145 genes expression was altered after MCAO surgery, of which 923 genes were up-regulated and 1222 genes were down-regulated. Additionally, 760 genes presented significantly differential expression in M2exo@DNase 1 group compared with MCAO group, including 512 upregulated and 248 downregulated genes (Fig. 7b). Kyoto encyclopedia of genes and genomes (KEGG) enrichment analysis of different expression genes among the three groups suggested that these genes were involved in several highly related pathways, including Toll-like, TGF-β, mTOR and tight junciton signaling pathways (Fig. 5c), which were mainly associated with immune response, infammatory process and cell survival. To better analyze the effects of altered genomic expression on cell behavior induced by MCAO surgery and M2exo@DNase 1 treatment, genes with significant differences were selected and grouped according to apoptosis, immunity, and inflammation. It was found that the proportion of promotional genes involved in these cell behaviors was remarkably increased after MCAO surgery, whereas generally suppressed by M2exo@DNase 1 treatment (Supplementary Fig. 20). The results suggest that M2exo@DNase 1 produced anti-apoptotic, immune activation inhibition and anti-inflammatory effects for stroke therapy.

Then altered genes with significant differences related to pathology of stroke were selected for heat map analysis (Fig. 5e). Encouragingly, M2exo@DNase 1 induced overexpression of Cdk4 and Id4, which mediate positive regulation of pro-angiogenesis[25,26] and were downregulated after MCAO surgery. Jun, Fos, Dusp1, and Tnfrsf12a that play important roles in promoting inflammation were significantly inhibited after

therapy[27-30]. Besides, M2exo@DNase 1 blocked Cdkn1a and Traf6 that promoted apoptosis[31,32]. The proposed mechanism of M2exo@DNase 1 therapy was shown in Fig. 5e. NETs disruption by DNase 1 and migcrogila polarization by M2exo led to BBB remodeling, inflammation alleviation and neurological protection through promoting the tight junction and TGF-β signaling pathways while blocking the mTOR and Toll-like signaling pathways. To verify the reliability of the mechanism, representative genes of each signaling pathways were tested by PCR. Consistent with the transcriptomic analysis, the results revealed significant upregulation of Cdk4, Id4 and Stradb, and downregulation of Jun when comparing M2exo@DNase 1 group with MCAO group (Fig. 5f).

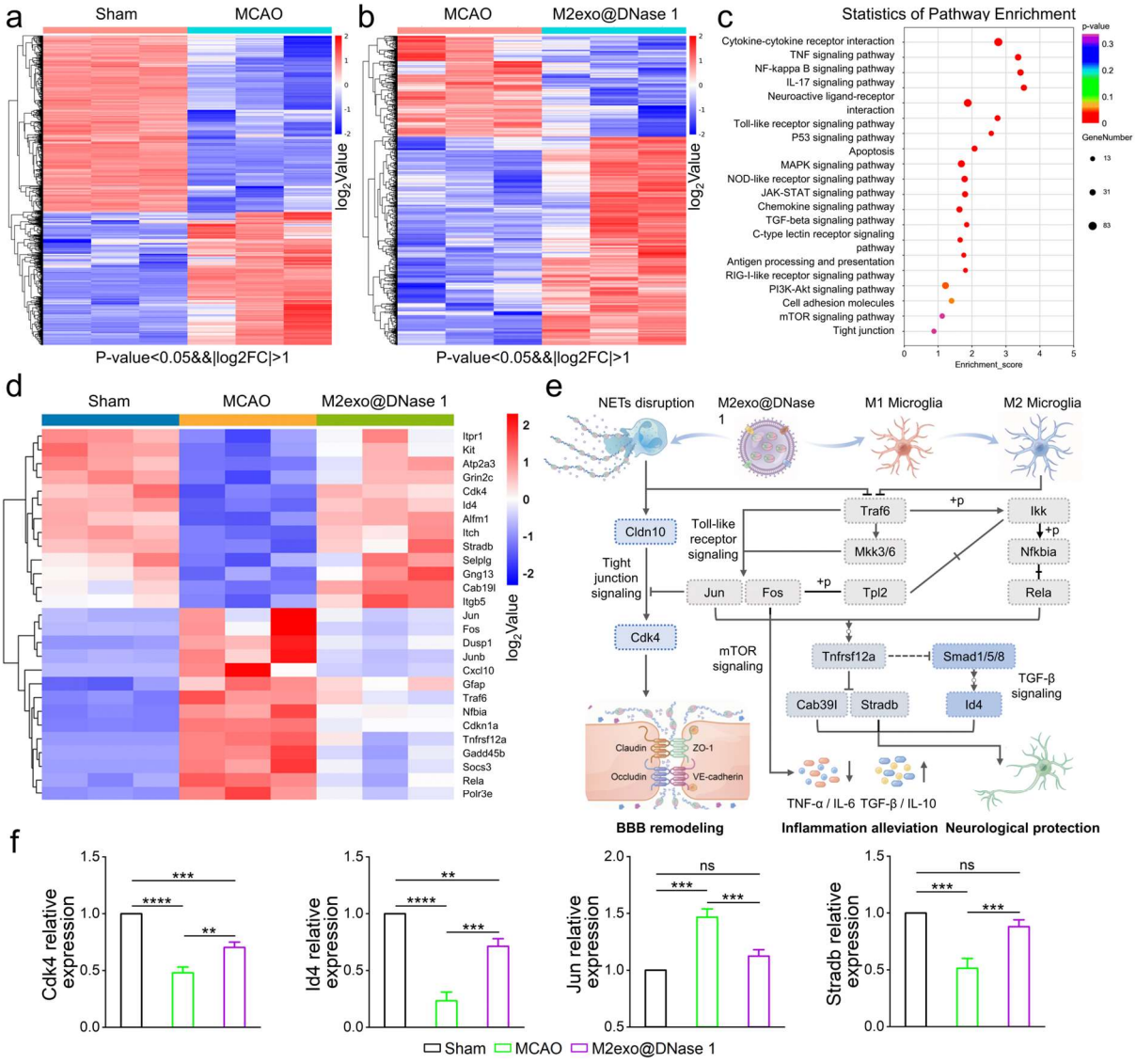

Fig. 7 Transcriptomic gene analysis. a,b Heatmap of transcriptome changes between **(a)** Sham and MCAO groups or **(b)** MCAO and M2exo@DNase 1 groups. **c** KEGG enrichment analysis of the top 20 genetic pathways based on M2exo@DNase 1 treatment. **d** Heatmap showing the relative changes in expression levels for selected genes. **e** Schematic illustration of the signaling pathway involved in M2exo@DNase 1 therapy for stroke. **f** qRT-PCR analysis of Cdk4, Id4, Jun and Stradb in different groups.

Toxicity evaluation. The systematic toxicity of M2exo@DNase 1 was evaluated by H&E staining and blood routine test in mice. No pathological changes of major organs including heart, liver, spleen, lung, and kidney were observed in all treatment groups (Supplementary Fig. 21). Blood routine (i.e. white blood count (WBC), lymphocyte (LY), monocyte (MON), granulocyte (Gran), red blood cell count (RBC), platelet count (PLT), hemoglobin (Hb)) were tested. Compared with Sham group, the blood routine levels of MCAO group were increased or decreased due to the inflammation and immune reponse poststoke. Generally, M2exo@DNase 1 treatment recovered the indexes within the normal range. Thus, the histopathology and hematology results verified that M2exo@DNase 1 have good biocompatibility and could be applied as a safe drug delivery system.

Discussion

NETs are highly associated with vascular damage and promotes inflammation after ischemic stroke. Studies have shown that DNase 1 can effectively inhibit NETs for vascular remodeling and inflammation alleviation[33,34]. Given the easily-lost activity of DNase 1 and the BBB obstacle, nanocarriers that can simultaneously remain the enzyme activity and cross the BBB may improve the therapeutic effect of DNase 1. As naturally occurring nanocarriers, exosomes are well tolerated and have minimal non-specific interactions in vivo, leading to prolonged blood circulation of cargo[35]. In particular, exosomes derived from macrophages can cross the BBB with approximately 5-fold increased accumulation in inflamed brain when comparing with the healthy brain[36]. Additionally, M2 macrophage-derived exosomes have been proved to attenuate neuronal apoptosis poststroke via exosomal miR-124, which modulates M2 polarization in

microglia and exerts anti-inflammatory effect on injured neurons[37,38]. In this work, we proposed M2 exosome-medicated drug vector for the ischemic brain-selective delivery of DNase 1 to achieve enhanced stroke therapy through synergistic effect of NETs depletion and microglia polarization. Our DNase 1-loaded M2 exosomes have been proved to effectively traffic to ischemic hemisphere, overcoming the limitation of BBB obstacle (Fig. 3a-c).

Ischemic injury triggers the recruitment of neutrophils, release of ROS, and activation of microglia, which further leads to the release of proinflammatory chemokines and cytokines[39]. It is well documented that neutrophils are the first group of cells that aggregate towards the infarct brain, then release NETs upon ROS stimulation and inflammatory factors[40]. We have demonstrated that neutrophils and NETs were abundantly accumulated at the peri-infarct cortex of mice brains at day 3 after MCAO surgery (Fig. 5c-e). Interestingly, M2exo@DNase 1 treatment could greatly reduce NETs formation in the infarct brain but not neutrophils (Fig. 5e-g). Apart from the NETs depletion by DNase 1, M2exo-mediated phenotypic polarization of microglia from M1 to M2 type produces anti-inflammatory cytokines, further alleviating the ischemia-reperfusion injury (Fig. 5a, b).

Owing to the synergistic effect of NETs inhibiton and microglia polarization, M2exo@DNase 1 dramatically shrank the brain lesion area of mice, reducing 71.2% of infarct volume compared with MCAO group (Fig. 3f, g). In addition, the assessment of long-term neurological functional outcome revealed that M2exo@DNase 1 promoted motor and cognitive function recovery of stroke mice (Fig.4 a-k). It has been reported that NETs are involed in BBB breakdown, and disruption of NETs can maintain vascular integrity[24]. Encouragingly, M2exo@DNase 1 signifcantly reduced BBB breakdown with enhanced efficiency compared to DNase 1 alone (Fig. 6a-f). The superior BBB remodeling ability of our DNase 1-loaded M2 exosomes can be attributed to targeted delivery of DNase 1 towards ischemic brain along with the anti-inflammation effect of M2 exosomes. Considering the similar pathological process of incuction by inflamation and immune response in various ischemic injuries, the DNase 1-loaded M2 exosomes may be applicable to other organ systems, such as heart, liver and kidneys. Additionally, transcriptomic gene analysis illustrated the mechanism of M2exo@DNase 1 threatment. NETs disruption by DNase 1 promoted

BBB remodeling through upregulation of tight junction signaling pathway. On the other hand, the synergistic effect of the nanoplatform blocked Toll-like signaling pathway in the intrinsic immune system, which inhibited the secretion of inflammatory factors and subsequently activated TGF-β signaling to promote nerve cell regeneration. Simultaneously, downregulation of Toll-like signaling led to inhibiton of mTOR signaling pathway, suppressing autophagy and apoptosis of neuronal cells.

Despite the encouraging therapeutic effect of M2exo@DNase 1, it should be mentioned that some limitations also exist in the design of this system. Firstly, the M2 exosomes cannot ensure the targeted delivery of DNase 1 by crossing BBB. To increase BBB targeting, ligands can be attached to M2exo, either by direct covalent conjugation[41] or through recombinant expression of fusion protein enriched in exosomal membranes[42]. Secondly, great efforts still need to be paid for the clinical translation of exosomal system due to the expensive scale-up and long-term stability of the biological carriers. Nevertheless, these limitations cannot overshadow the brilliance of M2exo@DNase 1.

In summary, we developed a M2 macrophage-derived exosomal system to enhance BBB penetration of DNase 1 for combined therapy of ischemic stroke. The detailed in vivo results have authenticated that M2exo@DNase 1 not only effectively overcomes the BBB obstacle and improves the delivery efficiency of cargo to the infarct brain, but also significantly attenuates neuroinflammation and modulates immune response via disruption of NETs and M2 polarization of microglia. By taking advantages of these strategies, M2exo@DNase 1 effectively reduces brain infaction, improve neurologic outcome, and promotes BBB remodeling. This nanoplatform provides an efficient and generalizable avenue for ischemic stroke therapy and opens new doors for the future successful clinical translation of nanomedicine.

Methods

Macrophage polarization. RAW264.7 (Chinese Academy of Sciences) were cultured in DMEM medium (Gibco) with 1% penicillin streptomycin (HyClone) and 10% fetal bovine serum (FBS, Biological Industries) at 37 °C with 5% CO_2. To polarize RAW264.7 to M2 phenotype, serum exosomes were removed by centrifugation at 15000×g for 120 min, and IL-4 (20 ng/mL, Sigma-Aldrich) was added

to the culture medium for 24 h. To test the polarization efficiency, macrophages were labeled with CD11b-FITC (1:100, Abcam), CD206-PE (1:100, eBioscience) and CD80-PE (1:100, Abcam) for flow cytometry analysis.

Collection of exosomes. The culture medium was first centrifuged (3500×g, 15 min) to remove cells, apoptotic bodies and cell fragments. Then the supernatant was centrifuged (2500×g, 15 min) by ultrafiltration tube (Millipore, UFC910096) to collect the concentrate, followed by filtering to remove particles above 450 nm. Finally, the filtrate was centrifuged at 12000×g for 120 min (Beckman Optima XE-90) and filtered (diameter 220 nm) to obtain M2-phenotype exosomes (M2exo), which were resuspended in PBS. All operations were performed under aseptic at 4 ℃.

Preparation of M2exo@DNase 1. 10 μL of M2exo, 40 μL of DNase 1 (100 U, Sigma-Aldrich) and PBS buffer were added into the electroporation dish (Biorad 1652088) under the condition of 250 V and 350 μF (Biorad Gene Pulser Xcell). The mixture was incubated at 37 ℃ for 30 min to restore the membrane of M2exo, subsequently centrifuged to obtain M2exo@DNase 1.

Characterization of M2exo@DNase 1. The particle size and zeta potential of M2exo@DNase 1 were measured by Malvern Zetasizer Nano ZS90. The morphology of M2exo and M2exo@DNase 1 were observed using transmission electron microscopy (TEM, JEM-2100F). Briefly, 10 μL of exosomes was added onto ultra-thin carbon film (300 meshes) and dried for 10 min. Then 10 μL of 1% phosphotungstic acid (pH = 7) was added to the film for 10 min staining, and imaged by TEM.

Protein concentration measurement. The protein concentration of M2exo was measured using the Komas Brilliant Blue method. Briefly, the standard protein (Sigma-Aldrich) diluted in a concentration gradient was added sequentially to a 96-well plate, followed by the addition of 200 μl of Thomas Brilliant Blue (Sigma-Aldrich) for 20 min reaction. The mixture was detected by enzyme marker (Biotek ELX800) to establish standard protein curve through the absorbance at 595 nm. The protein concentration of M2exo was determined according to the standard curve.

Protein composition measurement. The protein compositions of RAW264.7 membrane, M2exo and M2exo@DNase 1 were measured by SDS-PAGE (BG-Power600 Power Supply). Briefly, RAW264.7 membrane, M2exo and M2exo@DNase 1 with equal protein concentrations were heated in 95 ℃ water bath for 5min for denaturation, added into SDS-PAGE electrophoresis system to separate the gel.

Enzymatic activity. DNase 1 hydrolase activity C (U/mL) was detected according to GB/T 34801-2017 (the national standard of the People's Republic of China for the assay of deoxyribonuclease activity). M2exo@DNase 1, HAc-NaAc (0.1 mol/L, pH = 5, Sigma-Aldrich) and calf thymus DNA (Sigma-Aldrich) solutions were mixed in a certain proportion. The absorbance of the mixture at 260 nm (Δ^{A26}) was tested under ultraviolet spectrophotometer. The enzyme activity was calculated according to formula 1 (where f = dilution multiple), the DNase 1 loading efficiency (LE) was calculated as formula 2, and the DNase 1 loading content (LC) was calculated as formula 3.

$$C = \frac{\Delta^{A260} \times 1000 \times f}{10} \quad (1)$$

$$\mathrm{LE}\ (\%) = \frac{\text{Enzyme activity in exo C (U/mL)}}{\text{Feeding enzyme activity C (U/mL)}} \times 100 \quad (2)$$

$$\mathrm{LC\ (U/mg)} = \frac{\text{Enzyme activity in exo C (U/mL)}}{\text{Protein concentration in exo c (mg/mL)}} \quad (3)$$

Microglia polarization. To investigate the ability of in vitro microglia polarization by M2exo, the oxygen glucose deprivation/reoxygenation (OGD/R) model was applied to simulate ischemic stroke injury. Briefly, 2×10^5 BV-2 (Chinese Academy of Sciences) were inoculated in confocal dishes with DMEM medium containing 1% penicillin streptomycin and 10% FBS at 37 ℃ with 5% CO_2. 24 h later, the culture condition was changed to glucose-free and serum-free medium (Gibco) with 95% N_2 and 5% CO_2 to simulate a hypoxic environment. 3 h later, the cells were cultured in normal medium with 5% CO_2 for another 24 h to simulate reperfusion injury, followed by treated with different formulations for 24 h

and labeled with IBA-1-FITC (1:100, Abcam), CD206-PE (1:100, eBioscience) and CD16/32-PE (1:100, Abcam) for flow cytometry analysis.

Extraction and identification of neutrophils. Neutrophils were extracted from the bone marrow of adult C57BL/6 mouse. Briefly, the mouse bone marrow was suspended in 1640 medium (Gibco) with 10% FBS and filtered to make neutrophil suspension. Then, 4 mL of cell separation solution (Solarbio, P8550) A, 2 mL of solution C and the cell suspension were added to a centrifuge tube in order. The mixture was centrifugated (1000×g, 30 min) to collect the middle layer, which was added to erythrocyte lysis solution and washed for three times (250×g, 10 min) to collect the neutrophil suspension. All operations were performed under sterile condition. The extracted neutrophils were first identified by Wright's stain, showing multinucleated cell structure. To further investigate the purity of the extracted neutrophils, the cell suspension was labeled with CD45-PE (1:100, Abcam), CD11b-FITC (1:100, Abcam) and Ly6G-APC (1:100, Abcam), subsequently analyzed by flow cytometry.

Wright's stain of neutrophils. To identify the extracted neutrophils, the cell suspension was added to a slide and dried, then stained with Wright's staining solution (Solarbio) and fixed for 1 min, washed and imaged under the bright field of fluorescence microscope (Axio Observer Z1, Zeis, Germany).

Characterization of NETs[43]. To induce the release of neutrophil extracellular network (NETs), neutrophils were treated with phorbol 12-myristate 13-acetate (PMA, 20 ng/mL, Sigma-Aldrich) for 6 h. Then the cells were fixed with 4% paraformaldehyde at 4 ℃ for 10 min, and separately incubated with rabbit anti-H3cit (1:1000, Abcam) at 4 ℃ overnight and Alexa fluor 488 conjugated donkey anti-rabbit (1:1000, Invitrogen) for 1 h. The nuclei were stained with DAPI (1:1000, Sigma-Aldrich). Images were taken using confocal microscope (A1R+, Nikon).

In vitro NETs decomposion. After PMA induction, neutrophils were treated with PBS, DNase 1 and M2exo@DNase 1 with enzyme concentration of 100 U for 30 min. Then neutrophils were fixed with 4% paraformaldehyde at 4 ℃ and stained with SYTOX Green (1:500, S7020, Invitrogen), subsequently

observed by fluorescence microscope (Axio Observer Z1, Zeis, Germany). To quantitatively detect the NETs decomposion, the cells were determined by microplate reader (Varioskan LUX, Thermo Fisher Scientific, United States) at the absorbance of 488 nm.

NETs, eDNA and NE determination. To quantify the production of NETs, eDNA and NE from neutrophils, the cell supernatant was collected and measured with mouse NETs enzyme-linked immunosorbent assay (ELISA) kit (Jianglai biology), animal tissue DNA isolation kit (Foregene) and mouse neutrophil elastase (NE) ELISA kit (Mlbio), respectively.

MCAO model. Male C57BL/6 mice (8-12 weeks, 25-30 g) purchased from Beijing Huafukang Biotechnology Co., Ltd. were randomly divided into 5 groups. To establish the middle cerebral artery occlusion (MCAO) model, mice were first anesthetized with 5% isoflurane and maintained under 1.5% isoflurane after deep anesthesia. Then the neck skin of the mice was cut off and a silicon suture (Xinong Technology) was inserted from the right common carotid artery (CCA) into the internal carotid artery (ICA) at a depth of 8-10 mm. The successful construction of MCAO model was confirmed by the laser speckle contrast imaging system (RFLSI III, RWD) with more than 80% decrease in regional cerebral blood flow (rCBF). 60 min later, reperfusion was achieved after removal of the silicon suture. The procedure for the sham-operated group was similar to the model group except the insertion of the silicon suture. All animal experiments were conducted in accordance with Southwest Jiaotong University approved guidelines for the care and use of laboratory animals.

Near-infrared fluorescence imaging. To evaluate the brain-targeting ability of exosomes, MCAO mice were intravenously injected with the near-infrared fluorescent dye ICG and ICG-loaded M2exo (M2exo@ICG), respectively. Then mice were anesthetized with 5% isoflurane and imaged using near-infrared fluorescence in vivo imaging system (IVIS Spectrum) at predetermined time intervals (1 h, 3 h, 6 h and 12 h). To investigate the biodistribution of ICG and M2exo@ICG in MCAO mice, tissues including heart, liver, spleen, lung, kidney and brain were collected 12 h post injection for imaging.

Laser speckle flowmetry characterization. The rCBF (regional cerebral blood flow) of MCAO mice was monitored 1 h and 3 days post-surgery to evaluate the blood reperfusion after treatment. The scalp of mice was cut open to expose the skull and observed under laser speckle contrast imaging system.

TTC staining. To evaluate the brain infarction, triphenyltetrazolium chloride (TTC) staining was applied. At 3 days after MCAO surgery, mice were sacrificed to excise brains, which were frozen at - 20 °C for 20 min and cut into 2 mm thick slices, subsequently stained with 2% TTC (Solarbio) solution for 30 min. Images were processed with ImageJ software. The brain infarct volume was calculated as formula 4.

$$\text{Infarct volume (\%)} = \frac{\text{Contralateral hemisphere volume} - \text{Noninfarct ipsilateral hemisphere}}{\text{Contralateral hemisphere volume}} \times 100 \quad 4$$

Brain water content test. To study the effect of different groups on cerebral edema, the infarct brains of mice were excised after treatment and weighed to record the wet weight. The brains were then freeze-dried and weighed to record the dry weight. The water content of the brain was calculated as formula 5.

$$\text{Water content (\%)} = \frac{\text{Wet weight} - \text{Dry weight}}{\text{Wet weight}} \times 100 \quad 5$$

Magnetic resonance imaging (MRI). At 3 days, 7 days, 14 days and 28 days post MCAO surgery, mice were placed into the MRI machine, then anesthetized with 5% isoflurane and maintained under 1.5% isoflurane during the test. MRI scanning was conducted on small animal 7T magnetic resonance scanning system (Bruker, BioSpec 70/30USR). The T2-weighted series used are as follows: TR = 2,500.0 ms, TE = 35.0 ms, flip angel = 90.0°, NEX = 4, FOV = 3.00 cm, matrix = 256, section thickness = 1.00 mm, scan = 20, echo =1/1[44]. Images were processed with the ImageJ software.

H&E, NISSL and LBF staining. To evaluate the brain infarction by immunohistochemistry, mice were sacrificed 3 days after MCAO surgery to collect brain tissues, which were cut into 3 μm sections for hematoxylin-eosin (H&E), NISSL and luxol fast blue (LBF) staining. The sections were observed under microscope slide scanner (PANNORAMIC MIDI, 3DHISTECH).

Behavioral test. To investigate the long-term motor and cognitive functions of MCAO mice after treatment, a series of behavioral tests were performed within 28 days. Rotarod test, adhesive test, balance beam test and Barnes maze test were performed three times a day[45]. The cylinder test was performed once on each test day. The modified neurological severity score (mNSS) has a total of 18 points, including 6 points for the motor test, 2 points for the sensory test, 6 points for the beam balance test, and 4 points for reflex loss and abnormal movement.

Rotarod test. This test is used to assess motor function after stroke. Mice were placed on a rotating rod with accelerating speed from 5 to 20 turns per minute. The mean time to stay on the rod was recorded as the latency to fall. Mice were trained three times a day for 5 days prior to the MCAO surgery.

Cylinder test. This test is used to assess forepaw use and rotational asymmetry. Mice were placed into a transparent cylinder (height: 15 cm; diameter: 9 cm), and a video camera was used to record the contact of the forepaw with the cylinder for 10 min. The asymmetry rate was calculated as formula 6.

$$\text{Asymmetry rate } (\%) = \frac{\mathrm{L} - \mathrm{R}}{\mathrm{L} + \mathrm{R} + \mathrm{B}} \times 100 \qquad 6$$

L: the number of left forepaw contacts, R: the number of right forepaw contacts, B: the number of both contacts.

Adhesive test. This test is used to evaluate the tactile response and sensorimotor function. A 3×3 mm^2 sized patch was attached to the paralyzed forepaw of MCAO mice. The time for the mice to successfully remove the patch was recorded.

Barnes maze test. This test is used to assess memory function after stroke. Mice were placed on a circular platform surrounded by 20 hole and exposed to bright light above the platform. A dark box underneath one of the holes was the escape hole. The time for the mice to enter the escape hole was recorded and their movements were analyzed by the SMART 3.0 behavioral recording system (Panlab, Spain). Mice were trained three times a day for 5 days prior to the MCAO surgery.

Immunofluorescence. To perform immunofluorescence staining, brains were separated from mice at day 3 after MCAO and made into 20 μm frozen coronal sections. The first antibodies included rat anti-

CD16/32 (1:200, Abcam), rabbit anti-CD206 (1:100, Abcam), rat anti-Ly6G (1:200, Abcam), rabbit anti-GFAP (1:1000, Abcam), rabbit anti-H3cit (1:1000, Abcam). The secondary antibodies included Alexa Fluor 647-conjugated goat anti-rat IgG (1:1000, Abcam), Alexa Fluor 488-conjugated goat anti-rat IgG (1:1000, Abcam), Alexa Fluor 488-conjugated goat anti- rabbit IgG (1:1000, Servicebio), and Alexa Fluor 647-conjugated goat anti- rabbit IgG (1:1000, Servicebio). The staining sections were observed using Ortho fluorescence microscope (Beijing Shiji Kexin Scientific Instrument Co., Ltd).

In vivo microglia polarization. To quantitatively detect the microglia polarization in the ischemic area, the infarct half brain was homogenized and labeled with IBA-1-FITC (1:100, Abcam), CD206-PE (1:100, eBioscience) and CD16/32-PE (1:100, Abcam) for flow cytometry analysis.

Western blotting. To detect the protein expression of the infarct brain, the tissues were first lysed by RIPA buffer and measured by BCA protein analysis kit. The equal amount of protein (20 μg) was added to sodium dodecyl sulfate-polyacrylamide gel electrophoresis (SDS-PAGE). Then the gel was transferred to PVDF membrane and incubated with primary antibodies including H3cit (1:800, Abcam), STING (1:800, Abcam), VE-Cadherin (1:800, Abcam), Claudin-5 (1:800, Abcam), Occludin (1:800, Abcam) and ZO-1 (1:800, Abcam) at 4 ℃ overnight. Afterwards, the membrane was incubated with horseradish peroxidase (HRP)-conjugated secondary antibodies at room temperature for 1 h, followed by reacting with the enhanced chemiluminescence substrate. The proteins bands were imaged by chemiluminescence imager (Monna, QuickChemi 5100) and processed with ImageJ software.

Evans blue (EB) staining. To evaluate the permeability of blood-brain barrier (BBB) in mice, 200 μL of EB (2%, Sigma-Aldrich) solution was intravenously injected 24 h post MCAO. 2 h later, the brains were separated for photographing. To quantify the EB concentration, the brains were weighed and homogenized in 4 mL of dimethylformamide. Then the homogenate was incubated at 37 ℃ for 48 h and centrifuged (10000 rpm, 20 min) to collect and the supernatant. The content of EB was determined by measuring the absorbance of supernatant at 632 nm.

In vivo vascular imaging. MCAO mice were placed in the induction chamber and anesthetized to create cranial windows for two-photon confocal microscopy (A1RMP＋, Nikon) observation. Briefly, the mice skull was opened by high-speed micro drill at somatosensory cortex, then fixed with sterile cover glass and dental cement[8]. To investigate the neutrophil infiltration, 100 μL of FITC-dextran (10 mg/mL, 2000 KDa, Sigma-Aldrich) and Ly6G-APC (5 μg, Abcam) were injected into the caudal vein. To evaluate the vascular penetration, 100 μL of FITC-dextran (10 mg/mL, 40 KDa, Sigma-Aldrich) was injected into the caudal vein. Images were obtained by Z-stack scanning from 200 μm to 500 μm below the cortical surface. Images were analyzed and processed using NIS-Elements Viewer 4.20 and ImageJ software[46]. Then the mice were sacrificed to excise the brains, which were made into frozen sections for further fluorescence imaging.

Transmission electron microscope. To investigate the damage of BBB in infarct area, the brain was fixed with 3% glutaraldehyde and postfixed in 1% osmium tetroxide, dehydrated in series acetone, infiltrated in Epox 812 for a longer, and embedded. The semithin sections were stained with methylene blue and ultrathin sections were cut by diamond knife, stained with uranyl acetate and lead citrate. Sections were examined with JEM-1400-Flash Transmission Electron Microscope.

Histocompatibility and blood compatibility. To analyze the biocompatibility of exosomes, organs including heart, liver, spleen, lung, kidney, and blood were collected 3 days after MCAO. HE staining and blood routine test were performed, respectively. CaseViewer was used for image analysis and processing.

ELISA test. To detect cytokines in the macrophage cell supernatant and brain tissues, enzyme-linked immunosorbent assay (ELISA) method was performed. Elisa kits included mouse TNF-α elisa kit (Solarbio), mouse IL-6 elisa kit (Solarbio), mouse IL-10 elisa kit (Solarbio), mouse TGF-β elisa kit (Solarbio), mouse myeloperoxidase (MPO) elisa kit (Solarbio), mouse IL-1β elisa kit (Solarbio), mouse super oxidase dismutase (SOD) elisa kit (CUSABIO), mouse glutathione peroxidase (GSH-Px) elisa kit (CUSABIO).

Transcriptome analysis. The infarct brains of mice at 3 days after MCAO was separated for RNA extraction and quantified using NanoDrop 2000 spectrophotometer (Thermo Scientific, USA). RNA integrity was analyzed by Agilent 2100 Bioanalyzer (Agilent Technologies, Santa Clara, CA, USA). Then the libraries were constructed using TruSeq Stranded mRNA LT Sample Prep Kit (Illumina, San Diego, CA, USA). The transcriptome sequencing and analysis were conducted by OE Biotech Co., Ltd. (Shanghai, China)[47].

qPCR analysis. To detect the expression levels of related genes, the infarct hemispheres of MCAO mice were collected at 3 days post stroke for polymerase chain reaction (PCR) analysis. The total RNA was extracted from tissues using RNA extraction reagent (TRIcom, Tianmu Biological), followed by reversely transcription into cDNA using AccuRT Genomic DNA Removal Kit) (abm) by 5X All-In-One MasterMix. Real-time quantitative PCR was performed on qPCR analyzer (FQD-96C, BIOER), and the results were processed using the ΔΔCT method. Primers are as follows:
JUN: TGGGCACATCACCACTACAC (forward), TCTGGCTATGCAGTTCAGCC (reverse). Cdk4: CTTAGCCGAGCGTAAGGCTG (forward), GGAGGTGCTTTGTCCAGGTA (reverse). Id4: CGATGGATGGCCAGGTGTG (forward), CTCCGGTGGCTTGTTTCTCT (reverse).

Stradb: CAGTGTTCACTGTTGGCAGC (forward), AGCTGACTTGCTGAACCGTA (reverse).
GAPDH: GGTTGTCTCCTGCGACTTCA (forward), TGGTCCAGGGTTTCTTACTCC (reverse).

The data were analyzed using the cycle threshold (Ct) value.

Statistical information. Statistical analysis was performed in Origin 2021 or with genomic software. For comparison of means of samples with normal distribution and homogeneous variance, an unpaired *t*-test was used for two groups. For samples with more than two groups, the one-way ANOVA method was used for multiple comparisons. Data are presented as mean ± SD. For all figures: ns, not significant; *, $P < 0.05$; **, $P<0.01$; ***, $P<0.001$; ****, $P<0.0001$.

Data Availability

Source data are provided with this paper. The authors declare that all other data supporting the findings of this study are available within the paper, Supplementary Information or Source Data file. Source data are provided with this paper.

References

1. Campbell, B.C.V. & Khatri, P. Stroke. *Lancet* **396**, 129-142 (2020).

2. Iadecola, C. & Anrather, J. The immunology of stroke: from mechanisms to translation. *Nat. Med.* **17**, 796-808 (2011).

3. Silvestre-Roig, C., Braster, Q., Ortega-Gomez, A. & Soehnlein, O. Neutrophils as regulators of cardiovascular inflammation. *Nat. Rev. Cardiol.* **17**, 327-340 (2020).

4. Papayannopoulos, V. Neutrophil extracellular traps in immunity and disease. *Nat. Rev. Immunol.* **18,** 134–147 (2018).

5. Daniel, C. *et al.* Extracellular DNA traps in inflammation, injury and healing. *Nat. Rev. Nephrol.* **15**, 559-575 (2019).

6. Mutua, V. & Gershwin, L.J. A Review of Neutrophil Extracellular Traps (NETs) in Disease: Potential Anti-NETs Therapeutics. *Clinic. Rev. Allerg. Immunol.* **61**, 194-211 (2021).

7. Huang, H. *et al.* Damage-associated molecular pattern–activated neutrophil extracellular trap exacerbates sterile inflammatory liver injury. Hepatology **62**, 600-614 (2015).

8. Kang, L. *et al.* Neutrophil extracellular traps released by neutrophils impair revascularization and vascular remodeling after stroke. *Nat. Commun.* **11**, 2488 (2020).

9. Gunzer, M. Escaping the traps of your own hunters. Science **358**, 1126-1127 (2017).

10. Denorme, F. *et al.* Neutrophil extracellular traps regulate ischemic stroke brain injury. *J. Clin. Invest.* **132**, e154225 (2022).

11. Li, C. *et al.* Neutrophil Extracellular Traps Exacerbate Ischemic Brain Damage. *Mol. Neurobiol.* **59**, 643-656 (2022).

12. Lan, X., Han, X., Li, Q., Yang, Q. W. & Wang, J. Modulators of microglial activation and polarization after intracerebral haemorrhage. *Nat. Rev. Neurol.* **13**, 420-433 (2017).

13. Yao, K. & Zu, H. Microglial polarization: novel therapeutic mechanism against Alzheimer's disease. *Inflammopharmacology* **28**, 95-110 (2020).

14. Xue, Y. *et al.* Microglial polarization: novel therapeutic strategy against ischemic stroke. *Aging Dis*. **12**, 466-479 (2021).

15. Zhang, Z.G., Buller, B. & Chopp, M. Exosomes — beyond stem cells for restorative therapy in stroke and neurological injury. *Nat. Rev. Neurol.* **15**, 193-203 (2019).

16. Betzer, O. *et al.* In Vivo Neuroimaging of Exosomes Using Gold Nanoparticles. *ACS Nano* **11**, 10883-10893 (2017).

17. Kim, H.Y. *et al.* Mesenchymal stem cell-derived magnetic extracellular nanovesicles for targeting and treatment of ischemic stroke. *Biomaterials* **243**, 119942 (2020).

18. Hou, Y. *et al.* The novel target：exosoms derived from M2 macrophage. *Int. Rev. Immunol.* **40**, 183-196 (2021).

19. Li, H. *et al.* M2-type exosomes nanoparticles for rheumatoid arthritis therapy via macrophage re-polarization. *J. Control. Release.* **341**, 16-30 (2022).

20. Wu, G. *et al.* Molecularly Engineered Macrophage-Derived Exosomes with Inflammation Tropism and Intrinsic Heme Biosynthesis for Atherosclerosis Treatment. *Angew. Chem. Int. Ed.* **59**, 4068-4074 (2020).

21. Wei, K. *et al.* M2 macrophage-derived exosomes promote lung adenocarcinoma progression by delivering miR-942. *Cancer Lett.* **526**, 205-216 (2022).

22. Hallez, C. *et al.* Hypoxia-induced human deoxyribonuclease I is a cellular restriction factor of hepatitis B virus. *Nat. Microbiol.* **4**, 1196-1207 (2019).

23. Raabe, A. *et al.* Laser Doppler imaging for intraoperative human brain mapping. *NeuroImage* **44**, 1284-1289 (2009).

24. Wang, R. *et al.* Neutrophil extracellular traps promote tPA-induced brain hemorrhage via cGAS in mice with stroke. *Blood* **138**, 91-103 (2021).

25. Balda , M.S., Garrett , M.D. & Matter , K. The ZO-1–associated Y-box factor ZONAB regulates epithelial cell proliferation and cell density. *J. Cell Biol.* **160**, 423-432 (2003).

26. Fontemaggi, G. *et al.* The execution of the transcriptional axis mutant p53, E2F1 and ID4 promotes tumor neo-angiogenesis. *Nat. Struct. Mol. Biol.* **16**, 1086-1093 (2009).

27. Tang, S. *et al.* Pivotal role for neuronal Toll-like receptors in ischemic brain injury and functional deficits. *Proc. Natl. Acad. Sci. U.S.A.* **104**, 13798-13803 (2007).

28. Bakiri, L. *et al.* Liver carcinogenesis by FOS-dependent inflammation and cholesterol dysregulation. *J. Exp. Med.* **214**, 1387-1409 (2017).

29. Bilchick, K. *et al.* Cardiac resynchronization therapy reduces expression of inflammation-promoting genes related to interleukin-1β in heart failure. *Cardiovasc. Res.* **116**, 1311-1322 (2019).

30. Qu, J. *et al.* Su1642 Bile Acids-induced Tnfrsf12a Expression Aggravates Cholestatic Liver Injury Through Promoting Hepatocyte Pyroptosis. *Gastroenterology* **158**, 1370-1371 (2020).

31. Lin, M. *et al.* Elevated P21 (CDKN1a) Mediates Apoptosis of Beta-Thalassemic Erythroid Cells in Mice but Its Ablation Doesn't Improve Erythroid Maturation. *Blood* **136**, 19 (2020).

32. Chen, H. *et al.* Blocking TRAF6 Function Domain by TRAF6 Dominant Negative (TRAF6dn) for Inhibition of Multiple Myeloma Cell Proliferative and Increase of Apoptosis through Regulation of NF-κB and JNK Pathways. *Blood* **108**, 3434 (2006).

33. Wang, S. *et al.* DNase-1 Treatment Exerts Protective Effects in a Rat Model of Intestinal Ischemia-Reperfusion Injury. *Sci. Rep.* **8**, 17788 (2018).

34. Josefs, T. *et al.* Neutrophil extracellular traps promote macrophage inflammation and impair atherosclerosis resolution in diabetic mice. *JCI Insight* **5**, e134796 (2020).

35. Nance, E., Pun, S.H., Saigal, R. & Sellers, D.L. Drug delivery to the central nervous system. *Nat. Rev. Mater.* **7**, 314-331 (2022).

36. Yuan, D. *et al.* Macrophage exosomes as natural nanocarriers for protein delivery to inflamed brain. *Biomaterials* **142**, 1-12 (2017).

37. Song, Y. *et al.* M2 microglia-derived exosomes protect the mouse brain from ischemia-reperfusion injury via exosomal miR-124. *Theranostics* **9**, 2910-2923 (2019).

38. Hamzei Taj, S., Kho, W., Riou, A., Wiedermann, D. & Hoehn, M. MiRNA-124 induces neuroprotection and functional improvement after focal cerebral ischemia. *Biomaterials* **91**, 151-165 (2016).

39. Eltzschig, H.K. & Eckle, T. Ischemia and reperfusion—from mechanism to translation. *Nat. Med.* **17**, 1391-1401 (2011).

40. Burn, G.L., Foti, A., Marsman, G., Patel, D.F. & Zychlinsky, A. The Neutrophil. *Immunity* **54**, 1377-1391 (2021).

41. Tian, T. *et al.* Surface functionalized exosomes as targeted drug delivery vehicles for cerebral ischemia therapy. *Biomaterials* **150**, 137-149 (2018).

42. Alvarez-Erviti, L. *et al.* Delivery of siRNA to the mouse brain by systemic injection of targeted exosomes. *Nat. Biotechnol.* **29**, 341-345 (2011).

43. Gavillet, M., Martinod, K., Renella, R., Wagner, D.D. & Williams, D.A. A key role for Rac and Pak signaling in neutrophil extracellular traps (NETs) formation defines a new potential therapeutic target. *Am. J. Hematol.* **93**, 269-276 (2018).

44. Feng, L. *et al.* Neutrophil-like Cell-Membrane-Coated Nanozyme Therapy for Ischemic Brain Damage and Long-Term Neurological Functional Recovery. *ACS Nano* **15**, 2263-2280 (2021).

45. Xia, Y. *et al.* Embryonic Stem Cell Derived Small Extracellular Vesicles Modulate Regulatory T Cells to Protect against Ischemic Stroke. *ACS Nano* **15**, 7370-7385 (2021).

46. Xu, H. *et al.* ADAMTS13 controls vascular remodeling by modifying VWF reactivity during stroke recovery. *Blood* **130**, 11-22 (2017).

47. Bolger, A.M., Lohse, M. & Usadel, B. Trimmomatic: a flexible trimmer for Illumina sequence data. *Bioinformatics* **30**, 2114-2120 (2014).

Acknowledgements

We thank Analytical and Testing Center of Southwest Jiaotong University. This work was supported by the National Key R&D Program of China (2021YFB3800900), the National Natural Science Foundation of China (51725303, 52033007, 2073236) and the Fifth China Association for Science and Technology Young Talent Support Project.

Author contributions

H.Q. and X.G. conceived the project. H.Q., Z.W. and X.G. designed the experiments and analyzed the results. Z.W. and R.L. performed confocal microscopy imaging. H.Q. and X.L. performed western blot assays and ELISA test. H.Q. and Z.W. performed the in vivo studies. R.L. and X.L. assisted immunfluoresecence and histological analysis. H.Q. and X.G. provived the transcriptomic gene analysis. The paper was written by H.Q., X.G. and S.Z.

Competing interests

The authors declare no competing interests.

Additional information

Supplementary information The online version contains supplementary material available at...

Correspondence and requests for materials should be addressed to X.G.

Supplementary Files

This is a list of supplementary files associated with this preprint. Click to download.

- SupplementaryInformation.pdf
- RS.pdf
- SupplementaryMovie1.mp4